doi:10.1093/brain/awz290 BRAIN 2019: 142; 3550–3564 | 3550

BRAIN
A JOURNAL OF NEUROLOGY

Traumatic microbleeds suggest vascular injury and predict disability in traumatic brain injury

Allison D. Griffin,[1,2] L. Christine Turtzo,[2] Gunjan Y. Parikh,[3,4] Alexander Tolpygo,[5] Zachary Lodato,[1,5] Anita D. Moses,[1,2] Govind Nair,[6] Daniel P. Perl,[1,7] Nancy A. Edwards,[8] Bernard J. Dardzinski,[1,7] Regina C. Armstrong,[1,7] Abhik Ray-Chaudhury,[8] Partha P. Mitra[5] and Lawrence L. Latour[1,2]

Traumatic microbleeds are small foci of hypointensity seen on T_2^*-weighted MRI in patients following head trauma that have previously been considered a marker of axonal injury. The linear appearance and location of some traumatic microbleeds suggests a vascular origin. The aims of this study were to: (i) identify and characterize traumatic microbleeds in patients with acute traumatic brain injury; (ii) determine whether appearance of traumatic microbleeds predict clinical outcome; and (iii) describe the pathology underlying traumatic microbleeds in an index patient. Patients presenting to the emergency department following acute head trauma who received a head CT were enrolled within 48 h of injury and received a research MRI. Disability was defined using Glasgow Outcome Scale-Extended $\leqslant 6$ at follow-up. All magnetic resonance images were interpreted prospectively and were used for subsequent analysis of traumatic microbleeds. Lesions on T_2^* MRI were stratified based on 'linear' streak-like or 'punctate' petechial-appearing traumatic microbleeds. The brain of an enrolled subject imaged acutely was procured following death for evaluation of traumatic microbleeds using MRI targeted pathology methods. Of the 439 patients enrolled over 78 months, 31% (134/439) had evidence of punctate and/or linear traumatic microbleeds on MRI. Severity of injury, mechanism of injury, and CT findings were associated with traumatic microbleeds on MRI. The presence of traumatic microbleeds was an independent predictor of disability ($P < 0.05$; odds ratio = 2.5). No differences were found between patients with punctate versus linear appearing microbleeds. Post-mortem imaging and histology revealed traumatic microbleed co-localization with iron-laden macrophages, predominately seen in perivascular space. Evidence of axonal injury was not observed in co-localized histopathological sections. Traumatic microbleeds were prevalent in the population studied and predictive of worse outcome. The source of traumatic microbleed signal on MRI appeared to be iron-laden macrophages in the perivascular space tracking a network of injured vessels. While axonal injury in association with traumatic microbleeds cannot be excluded, recognizing traumatic microbleeds as a form of traumatic vascular injury may aid in identifying patients who could benefit from new therapies targeting the injured vasculature and secondary injury to parenchyma.

1 Center for Neuroscience and Regenerative Medicine, Bethesda, Maryland, USA
2 Acute Cerebrovasular Diagnostics Unit of the National Institute of Neurologic Disorders and Stroke, Bethesda, Maryland, USA
3 R. Adams Cowley Shock Trauma Center, Program in Trauma, University of Maryland School of Medicine, Baltimore, USA
4 Division of Neurocritical Care and Emergency Neurology, Department of Neurology, University of Maryland School of Medicine, Baltimore, USA
5 Cold Spring Harbor Laboratory, Cold Spring Harbor, New York, USA
6 National Institute of Neurological Disorders and Stroke, Bethesda, Maryland, USA
7 Uniformed Services University of the Health Sciences, Bethesda, Maryland, USA
8 Surgical Neurology Branch of the National Institute of Neurological Disorders and Stroke, Bethesda, Maryland, USA

Correspondence to: Lawrence Latour, PhD
National Institute of Neurological Disorders and Stroke
National Institutes of Health

Received January 15, 2019. Revised July 15, 2019. Accepted July 28, 2019. Advance Access publication October 14, 2019
Published by Oxford University Press on behalf of the Guarantors of Brain 2019. This work is written by US Government employees and is in the public domain in the US.

10 Clinical Center Drive
Building 10, Room B1D733
Bethesda, MD 20892, USA
E-mail: LatourL@ninds.nih.gov

Keywords: radiological-pathological analysis; MRI biomarkers of traumatic brain injury; traumatic vascular injury; traumatic microbleeds; mild traumatic brain injury

Abbreviations: GCS = Glasgow coma scale; GOSE = Glasgow outcome scale – extended; GRE = gradient recalled echo; SWI = susceptibility-weighted imaging; TBI = traumatic brain injury; TMB = traumatic microbleed

Introduction

Approximately 2.5 million individuals were seen in emergency departments for traumatic brain injuries (TBIs) in the USA in 2013 (Taylor *et al.*, 2017), with more unaccounted for due to mild injuries not requiring immediate medical attention. While most patients with TBI recover completely within weeks to months of their injury, over 3 million individuals are living with TBI-related disability in the USA (Thurman *et al.*, 1999; Selassie *et al.*, 2008; Zaloshnja *et al.*, 2008). The lack of understanding of the underlying pathophysiology of TBI and heterogeneity of the injury has made it difficult to find factors other than severity of injury that reliably predict clinical outcome, particularly in patients with mild TBI. Discovery of biomarkers that can identify the underlying pathology of TBI in living patients would be useful for diagnosis, prognosis, identifying therapeutic targets, stratifying patients for clinical interventions, and improving patient outcomes.

MRI allows rapid and precise localization of macroscopic damage across the injured brain. Some imaging abnormalities, such as extra-axial haemorrhage, have direct implications for the management of patients. Other abnormalities seen in patients after TBI are more difficult to interpret or determine whether they are indicative of more severe underlying damage not visible on MRI. An example is the small, often punctate hypointensities observed on T_2*-weighted imaging, which have been observed in TBI patients after injury and in some cases found to correlate with clinical outcomes (Babikian *et al.*, 2005; Colbert *et al.*, 2010; Beauchamp *et al.*, 2013; Yuh *et al.*, 2013; Izzy *et al.*, 2017). On T_2*-weighted sequences, these traumatic microbleeds (TMBs) appear as punctate (Tong *et al.*, 2003; Huang *et al.*, 2015; Lawrence *et al.*, 2017) or linear (Ricciardi *et al.*, 2017) hypointensities secondary to the accumulation of ferromagnetic or paramagnetic substances, presumably originating from haemoglobin in blood or residual haemosiderin in the grey and white matter.

The literature surrounding TMBs in TBI is complicated by the wide range of terminology used to described them. For instance, they have been referred to as haemorrhagic diffuse axonal injury (Babikian *et al.*, 2005), foci of haemorrhagic axonal injury (Yuh *et al.*, 2013; Liu *et al.*, 2014), haemorrhagic traumatic punctate lesions (Geurts *et al.*, 2012; Spitz *et al.*, 2013), haemorrhage in supratentorial white matter on T_2*-weighted MRI (Iwamura *et al.*, 2012), T_2*-weighted lesions (Beauchamp *et al.*, 2013), cerebral microhaemorrhage (Colbert *et al.*, 2010), and TMBs (Toth *et al.*, 2016; Izzy *et al.*, 2017).

The clinical significance of TMBs is limited, in part, by the absence of radiological-pathological comparison to determine the cellular changes underlying signal abnormalities observed on MRI. While equating petechial blood seen on MRI to diffuse axonal injury (which is difficult to detect radiologically) may be appropriate in patients traditionally classified as severely injured, the association has yet to be established at the mild end of the spectrum of injury. The relationship is further confounded because the appearance of TMBs and severity of injury covary, making it difficult to determine whether TMBs are simply a signature of more severe injury or whether they could be causally associated with worse outcome. Additionally, studies have examined the prevalence of TMBs in patients during the chronic phase of disease where it can be difficult to distinguish them from non-traumatic microbleeds associated with small vessel disease (Conijn *et al.*, 2011), ageing (Fisher *et al.*, 2010) and ischaemic stroke (Naka *et al.*, 2004).

Previously, our group examined TMBs in the acute phase of TBI and stroke and found linear-appearing TMBs to be present only in patients with TBI, suggesting that at least linear TMBs are consistent with trauma and might be the result of injured vessels (Ricciardi *et al.*, 2017). Such linear TMBs are best visualized with the assistance of improved MRI parameters, including a 3D T_2*-weighted sequence, which can identify what initially appears to be punctate hypointensities on sequential axial slices to be connected in a linear shape. Based on the elongated appearance and frequent location and orientation similar to that of venous structures, we conjecture that TMBs seen on MRI may be a form of traumatic vascular injury distinct from primary injury to the axons.

During the conduct of an observational imaging-based study, a subject with linear TMBs detected in the hyperacute setting later expired, presenting an opportunity to study the pathology underlying a signature MRI finding in TBI patients. The aims of this study were to: (i) identify and characterize TMBs in a population of patients with acute and primarily mild TBI; (ii) determine whether the presence or type of TMB predicted patient outcomes; and (iii) characterize the pathology underlying TMBs in an index patient. We used MRI guided post-mortem sectioning

(Absinta *et al.*, 2014; Van Veluw *et al.*, 2013, 2015), 3D reconstruction of histological sections (Lee *et al.*, 2018), and post-mortem imaging methods to correlate pathological and radiological findings directly.

Materials and methods

This prospective study was approved by the Institutional Review Boards of the National Institutes of Health, Uniformed Services University of the Health Sciences and MedStar Washington Hospital Center, along with the Johns Hopkins Suburban Hospital Privacy Board. Written informed consent was obtained prior to all study procedures in accordance with the Declaration of Helsinki.

Patient population and study design

Patients presenting to the emergency department at level I (Medstar Washington Hospital Center) and level II (Johns Hopkins Suburban Hospital) trauma centres in the Washington, DC metropolitan area with (i) documented mechanism of trauma to the head; or (ii) suspicion of head injury concerning enough to trigger a CT for clinical purposes, were screened for enrolment in an observational protocol; the Traumatic Head Injury Neuroimaging Classification (THINC) study (clinicaltrials.gov NCT01132937). A multiphase screening approach under a HIPAA waiver of authorization was used by research staff to screen all patients presenting to the emergency department for suspected TBI to avoid investigator bias or exclude patients who lacked a clinical diagnosis of TBI (Cota *et al.*, 2018). Written informed consent was obtained from the patients or their surrogates prior to any study procedures. Inclusion criteria were as follows: (i) 18 years of age or older; (ii) deemed medically safe for participation; and (iii) consent and ability to obtain a research MRI within 48 h of injury. Patients were excluded if they were psychiatrically unstable or had any contraindication to MRI, including claustrophobia and pregnancy. For each year during the course of this study, ~4500 patients were screened for eligibility at two hospitals, 500 patients were approached for enrolment in the study and ~95 patients enrolled. Patients enrolled over a 78-month period were retrospectively selected for this analysis with the following criteria: (i) met the American Congress of Rehabilitation Medicine diagnostic criteria for TBI (Menon *et al.*, 2010); (ii) had a clinical CT of the head at presentation; and (iii) completed the research MRI at baseline with T_2^*-weighted image sequences that were interpretable.

Patients enrolled in this study were seen at up to four visits post-injury: (i) as soon as clinically permissible and $\leqslant$48 h; (ii) 1 week; (iii) 30 days; and (iv) 90 days. Research MRI at the hospital site, demographic information, emergency department intake measures [e.g. injury presentation; injury cause; evidence of loss of consciousness, altered mental status, and post-traumatic amnesia; Glasgow coma scale (GCS); injury symptoms assessed using the neurobehavioral symptom inventory (NSI); medications on admissions (including indication)] and history and risk factors were obtained during the first visit. A CT was obtained if medically necessary. Subsequent visits included a 3 T MRI, NSI, and clinical recovery assessment (Glasgow Outcome Scale-Extended, GOSE). For this analysis, we consider the imaging obtained at the baseline visit and outcomes obtained at the later available of 30- or 90-day visits.

Imaging protocol

Over the duration of the study, MRIs were acquired on three types of scanners: a 1.5 T (Signa, GE Medical Systems) or a 3 T (Skyra, Siemens) at Suburban Hospital, and a 3 T (Achieva, Philips) at MedStar Washington Hospital Center. The MRI protocol was standardized from commercially available sequences and consisted of a diffusion tensor imaging (DTI) sequence with derived isotropic diffusion-weighted imaging and apparent diffusion coefficient map, T_2^* gradient recalled echo (GRE), 'increased TE' T_2^* susceptibility-weighted imaging (SWI), T_2-FLAIR (fluid attenuated inversion recovery) and a 3D T_1-weighted sequence. Parameters of sequences were adjusted to produce similar appearing contrast across field strength. The total duration of this research MRI protocol was ~25 min. Additional parameters of T_2^*-weighted sequences can be found in Supplementary Table 1.

Classification of imaging findings

A neuroradiologist at each site interpreted all CT and MRI exams, resulting in a report used for clinical decision making. In addition, all magnetic resonance images were interpreted prospectively for research purposes, assessed for evidence of acute TBI, stratified as outlined previously by Ricciardi and colleagues (2017), and used for subsequent identification and analysis. TMBs were classified by presence of foci of hypointensity detected in the parenchyma first detectable on the GRE images, then confirmed on SWI series. We consider both traditional T_2^* gradient recalled echo, and higher resolution, 3D-T_2^* (sometimes referred to as SWI), with a longer echo time. Conspicuity of TMBs on MRI vary depending on the acquisition parameters. A conservative approach was taken to minimize the potential for overcalling where multiple contrast mechanisms (sequences) were reviewed to confidently identify and classify TMBs. Hypointense foci seen on SWI, but that could not also be confirmed on GRE, were not considered; i.e. to be classified as a microbleed, the lesion had to be visible on both scans when available. Other sequences, including high resolution 3D-T_1-weighted spoiled gradient recalled acquisition and T_2-FLAIR-weighted, were used to help confirm localization of TMBs localized to the parenchyma and specifically distinct from the extra-axial space. Following identification, TMBs were further stratified as either 'punctate' or 'linear' in appearance. Punctate TMBs were defined as circular appearing hypointensities seen in no more than two adjacent axial slices (i.e. $\leqslant$7 mm on T_2^* GRE), and further stratified as (i) any in number; or (ii) five or more in number (Fig. 1A–C). Linear TMBs were identified as linear-appearing hypointensities extending for more than two adjacent axial slices (i.e. $>$7 mm on T_2^* GRE). SWI images were reconstructed in tri-planar angled oblique (tri-planar view) using minimum intensity projection thin-slab of ~10 mm to aid in distinguishing linear from punctate classifications (Fig. 1D–F). Scans from one quarter of the population were independently interpreted by two raters to estimate inter-rater agreement using Cohen's kappa. Further, location of punctate

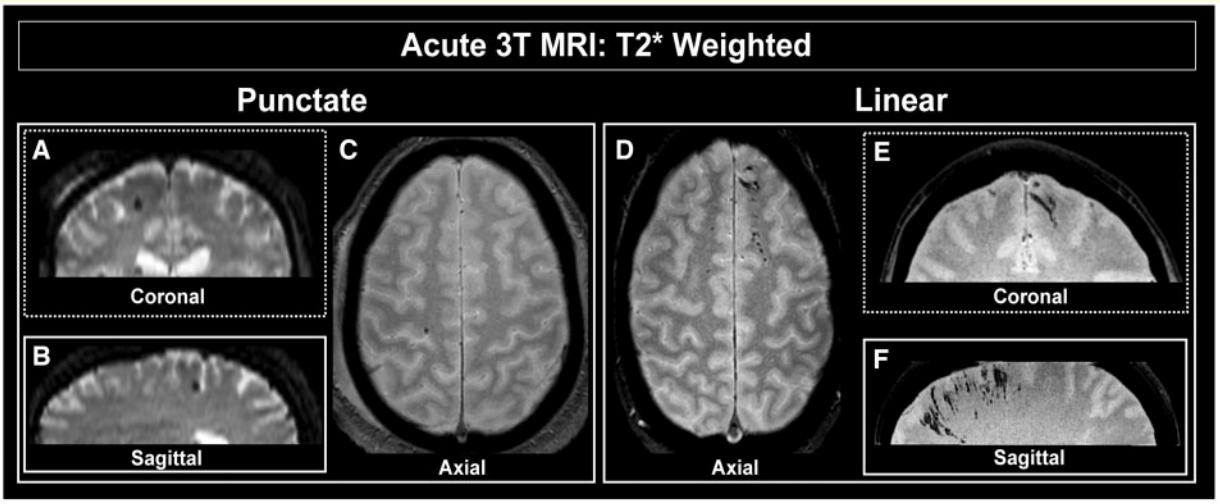

Figure 1 Characterization of TMBs in the clinical population. T_2*-weighted 3 T MRI of individual subject's brain to illustrate presence of TMBs. Coronal (**A**) and sagittal (**B**) views of representative punctate TMB shown in axial plane (**C**). Coronal (**E**) and sagittal (**F**) views of linear TMB shown in axial plane (**D**).

and linear TMBs were scored and included in research MRI interpretation. Specifically, location of linear or punctate TMBs were categorized as appearing in either the prefrontal, temporal, parietal and/or occipital lobe, as well as in deep or infratentorial regions of the brain.

Statistical analysis

We first compared patients with and without TMBs to identify demographic features, injury characteristics, clinical presentation, cardiovascular risk factors and medications (which categorically included anticoagulants, antiplatelets, antihypertensive agents, and lipid lowering agents), and other imaging factors that may be predictive of their presence. In the subgroup of patients with GOSE available, we stratified patients as having good recovery (GOSE = 7 or 8) versus disability (GOSE $\leqslant$ 6). To determine clinical and demographic characteristics associated with disability after TBI, a binary logistic regression was performed. Included in the model were parameters determined to be significant in the univariate analysis including: trauma level, GCS, TBI diagnosis, time to MRI, parenchymal and/or extra-axial injury evident on CT, and presence of punctate TMBs, linear TMBs, or both (Supplementary Table 3). Statistical analyses were conducted in Statistical Product and Service Solutions (SPSS) 16.0. The accepted level of significance was $P < 0.05$.

Neuropathology case study

Index patient

To evaluate the underlying pathology of TMBs, we performed post-mortem MRI and histology on the brain of a patient imaged with magnetic resonance within 48 h of injury and having both punctate and linear-appearing TMBs. Upon death, the next of kin contacted the research team and expressed a willingness to donate the decedent's brain for research purposes. The donation presented a rare opportunity to target findings seen on acute *in vivo* research MRI with histology. Consent for unrestricted autopsy was obtained, the decedent was transported to the NIH Clinical Center, and the whole brain was procured through autopsy at a post-mortem interval of 21 h.

The patient was a middle-aged male found unresponsive after a bicycle accident, with a right subdural haemorrhage with marked midline shift seen on CT that prompted hemicraniectomy and evacuation within 2 h of injury, indicating severe TBI. Consent for participation was provided by a family surrogate. A 3 T MRI scan of the patient was obtained post-hemicraniectomy within 48 h of injury, and again at 1 week post-injury and 3 months post-injury. Multiple punctate and linear regions of hypointensity were conspicuous on T_2*-weighted surfaces in the bilateral frontal lobes and in other regions of the brain. The patient died 7 months post-injury due to complications from sepsis. The patient had a previous history of remote head trauma and substance abuse. Medical records were obtained to aid in evaluating factors that may have contributed to antemortem injury.

Post-mortem MRI

Following procurement, whole brain was suspended in 10% formalin within a net and using a 'string' ligated to the basilar artery. A 3 T MRI was obtained immediately to confirm the presence of TMBs. The brain was maintained in 10% formalin to fix for 2 weeks and then switched to 1% diluted formalin solution. The fixed brain was placed in a custom-made MRI compatible holder and saturated with fluorinated oil (Fomblin, Solvay Specialty Polymers) that does not contain hydrogen protons visible on MRI. A vacuum was pulled for 2 h with a 1/3 horsepower vacuum pump, the oil outgassed while bubbles were noted to rise to the surface. A CT was obtained to confirm air bubbles were not present in the sulci or tissue.

The brain in the holder was transferred to a whole-body 7 T MRI scanner (Siemens) and imaged with a 32-channel receiver coil for ~48 h. Two contrast mechanisms were used, a multi-echo T_2*-weighted (ME-GRE), and a FLASH inversion recovery T_1-weighted sequence. Because of the size of the data,

multiple thick slabs were used to cover the whole brain. The following parameters were used for the ME-GRE; repetition time = 60 ms, four echo times = 6.2, 12, 18 and 24 ms, field of view = 160 mm, 380 × 380 voxels for 420 µm in-plane resolution, 88 axial-oblique slices, 420-µm thick for a coverage of 37 mm S-I, flip angle = 10°, total acquisition time of 136 min.

MRI to pathology co-registration and histology

The previously acquired *in vivo* 3 T MRI was used to identify sections containing TMBs and sections negative for TMBs. The 7 T whole brain MRI was used to confirm the location of the region of interest containing TMBs or excluding TMBs, and guide sectioning. The brain was then sectioned into standard histology slide-size (~2 × 2 × 3 cm) blocks or large (~2 × 7.5 × 12.5 cm) blocks containing possible regions of interest. Each of the standard sized blocks were imaged in a small-bore 7 T MRI at 100-µm isotropic resolution to confirm localization. The following parameters were used for the small-bore 3D multi-gradient echo (T_2*-weighted) MRI sequence, repetition time = 50 ms, echo times = 5, 13, 21, 29 and 37 ms, NA = 10, field of view = 4.6 × 3.6 × 1.1 cm, matrix = 460 × 360 × 110, 100 µm isotropic in-plane resolution, with a total acquisition time of 297 min.

After MRI, tissue was blocked to fit onto standard large 3 × 5″ slides and standard 1 × 3″ slides. Eight blocks of tissue were obtained for histopathological analysis; one section targeted by MRI for absence of TMB (as a negative control) and seven targeted by MRI for presence of TMB. Of these, four blocks were processed using standard 2D histopathology methods and four were processed using tape-transfer histopathology, of which one blocked tissue was used for 3D reconstruction. Additional blocks were obtained and analysed using standard 2D histopathological analysis, one large-section block and three standard histology-sized (1 × 3″) blocks. Of these three blocks, one section was targeted by MRI as a more inferior section that was centimetres away from a TMB, and was used as a negative control. Blocked tissue was frozen and sectioned at 20 µm using a custom tape-transfer process, or paraffin embedded and sectioned at 8 µm (large format) or at 5 µm (standard 1 × 3′) using standard sectioning methods. Tissue was cryoprotected in grades of sucrose, embedded in Neg-50™ (optimum cutting temperature compound) and frozen in isopentane. Tape-transfer sectioning techniques were accomplished through the use of an adapted cryostat sectioning method that preserved spatial registry and allowed later 3D reconstruction of the sample (Pinskiy *et al.*, 2015). Alternating sections were then stained using Gallyas silver, Nissl, and Perls Prussian Blue (Turtzo *et al.*, 2013) and cover slips were mounted using DPX medium (Sigma-Aldrich). Additional sections were stained with haematoxylin and eosin and amyloid precursor protein (APP) and read by a neuropathologist for evidence of axonal injury. APP staining was done on a Leica Bond automated stainer using Amyloid Precursor Protein Polyclonal Antibody (Invitrogen PA1-37099, Thermo Fisher) at 1:100 dilution with citrate epitope retrieval. Slides were digitized using a digital slide scanner (NanoZoomer 2.0-HT; Hamamatsu Photonics) at 0.46 µm/pixel; raw images were converted to lossless JPEG2000 files producing a 3 TB dataset of 550 images per sample. A volumetric brain stack was created by aligning all images within a frame of reference, via 2D rigid transformations (Lee *et al.*, 2018). This aligned 3D stack was processed further to produce a reconstructed sagittal, axial, and maximum intensity projection in each plane.

Data availability

The authors confirm that the data supporting the findings of this study are available from the corresponding author upon reasonable request.

Results

Patient demographics and clinical characteristics

Four hundred and thirty-nine patients enrolled during a 78-month time period met the inclusion criteria (Supplementary Fig. 1) for initial analysis (Table 1). The population was 73% male with a median age of 46 [interquartile range (IQR): 29–58]. The most common cause of injury was road traffic accidents (47%), followed by incidental fall (37%) and violence or assault (11%). Most patients had mild TBI (83%); the average GCS score at time of admissions was 15 (IQR: 14–15). The median time from injury to initial research MRI was 16.86 h (IQR: 6.83–26.01). In our study population, MRI findings of acute trauma by TBI severity level included extra-axial haemorrhage, with subdural haematoma present in 23% (102/439) [mild = 22% (81/365); moderate = 23% (13/55); severe = 47% (9/19)]; epidural haematoma in 0.4% (2/439) [moderate = 0.4% (1/55); severe = 5% (1/19)]; and subarachnoid haemorrhage in 20% (92/439) [mild = 19% (69/365); moderate = 27% (15/55); severe = 42% (8/19)]. Contusion (intracerebral haematoma with oedema) was present in 14% (60/439) [mild = 9% (33/365); moderate = 29% (16/55); severe = 42% (8/19)].

Inter-rater agreement was strongest for presence/absence of TMB (κ = 0.80). Moderate agreement was found on the interpretation of punctate (κ = 0.73), >5 punctate (κ = 0.79) and linear (κ = 0.75) TMBs. During this initial analysis, approximately one-third of patients (134/430, 31%) showed evidence of punctate and/or linear TMBs on baseline 3 T MRI (Table 1). 27% of mild patients, 47% of moderate patients, and 58% of severe TBI patients had TMBs identified. Of the 134 patients identified with TMBs, 64 patients had both punctate and linear TMBs, 26 patients had linear only, and 44 patients had punctate only. Of the 108 patients with evidence of punctate TMBs (those with both punctate and linear and those exclusively punctate), 29 patients had >5 and 79 patients had <5 punctate TMBs. Within the population of

Table 1 Demographic and clinical characteristics of patients with traumatic microbleeds

	Total *n* = 439	Absence *n* = 305	Presence *n* = 134	*P*-value	$\chi 2$ (df)
Demographics					
Age					
18–30	121 (28%)	89 (29%)	32 (24%)	0.109	9.712 (3)
31–64	255 (58%)	179 (59%)	76 (57%)		
65+	63 (14%)	37 (12%)	26 (19%)		
Sex					
Male	320 (73%)	219 (72%)	101 (75%)	0.739	0.605 (2)
Race					
White	281 (64%)	190 (62%)	91 (68%)	0.118	4.270 (2)
African-American	122 (28%)	93 (30%)	29 (22%)		
Other	36 (8%)	22 (7%)	14 (10%)		
Emergency department intake					
Trauma level					
Level 1	208 (47%)	141 (46%)	67 (50%)	0.266	0.531 (1)
Level 2	231 (53%)	164 (54%)	67 (50%)		
Injury cause					
Road traffic accident	206 (47%)	144 (47%)	62 (46%)	**0.029**	10.805 (4)
Incidental fall	161 (37%)	103 (34%)	58 (43%)		
Other non-intentional Injury	18 (4%)	17 (6%)	1 (1%)		
Violence/assault	48 (11%)	38 (12%)	10 (7%)		
Other	6 (1%)	3 (1%)	3 (2%)		
GCS, *n*[*]	426	295	131		
15	294 (69%)	217 (73%)	77 (59%)	**0.021**	9.712 (3)
14	87 (20%)	52 (18%)	35 (27%)		
<13	45 (11%)	26 (9%)	19 (14%)		
TBI diagnosis					
Mild	365 (83%)	268 (88%)	97 (72%)	**0.001**	16.671 (2)
Moderate	55 (13%)	29 (9%)	26 (20%)		
Severe	19 (4%)	8 (3%)	11 (8%)		
Clinical CT					
CT	310 (71%)	250 (82%)	60 (45%)	**0.001**	62.058 (1)
Parenchymal haemorrhage	385 (88%)	280 (92%)	105 (78%)	**0.001**	15.601 (1)
Extra-axial haemorrhage	323 (74%)	257 (84%)	66 (49%)	**0.001**	58.689 (1)
Clinical risk factors					
Patient endorsed concomitant medications					
Anticoagulant	13 (3%)	9 (3%)	4 (3%)	1	0 (1)
Antihypertensive	80 (18%)	51 (17%)	29 (22%)	0.229	1.513 (1)
Antiplatelet	28 (6%)	14 (5%)	14 (10%)	**0.032**	5.349(1)
Lipid lowering	58 (13%)	34 (11%)	24 (18%)	0.066	3.713 (1)
Patient endorsed medical history					
Coronary artery disease	13 (3%)	9 (3%)	4 (3%)	1	0 (1)
Diabetes	37 (8%)	25 (8%)	12 (9%)	0.852	0.069 (1)
Hyperlipidaemia	94 (21%)	56 (18%)	38 (28%)	**0.023**	5.530 (1)
Hypertension	112 (26%)	75 (25%)	37 (28%)	0.552	0.447 (1)
Stroke	15 (3%)	9 (3%)	6 (4%)	0.405	0.658 (1)
Transient ischaemic attack	12 (3%)	7 (2%)	5 (4%)	0.525	0.722 (1)
Valvular disease	7 (2%)	2 (1%)	5 (4%)	**0.030**	5.612 (1)
Peripheral vascular disease	3 (1%)	1 (0%)	2 (1%)	0.222	1.861 (1)
Atrial fibrillation	10 (2%)	7 (2%)	3 (2%)	1	0.001 (1)

[a]GCS at time of arrival to emergency department (ED) was not documented for all patients. Percentages reflect sample size (*n* numbers) revealed in this row.
Significance (bold) was determined for any *P*-value < 0.05.

patients with punctate TMBs, locations were distributed as follows: 58 (54%) patients showed punctate TMBs in frontal lobe, 35 (32%) in the temporal lobe, 25 (23%) in parietal lobe and 21 (19%) patients showed evidence of punctate TMBs in deep structures. Of the 90 patients with evidence of linear TMBs, locations were distributed as follows: 68 (76%) patients had evidence of linear TMBs in the frontal lobe, 15 (17%) patients had linear TMBs in

the temporal lobe and 31 (34%) in the parietal lobe. Linear microbleeds were seen more frequently in the frontal and parietal lobes while no linear TMBs were observed in deep structures. Note, some patients showed evidence of punctate and linear TMBs that were observed in multiple locations.

Demographic variables (Table 1) including age (P = 0.109), sex (P = 0.739), race (P = 0.118) and ethnicity (P = 0.266) did not differ between patients with and without TMBs. Injury severity ($P < 0.001$), GCS at time of arrival (P = 0.021), injury cause (P = 0.029), and evidence of trauma on CT ($P < 0.001$) were all significantly associated with TMBs. Patients with TMBs had more severe injury and lower GCS compared to patients without TMBs. Cardiovascular risk factors, like patient-endorsed history of hyperlipidaemia (P = 0.023), valvular disease (P = 0.030), and concomitant use of antiplatelet medications (P = 0.032), and patient-endorsed history of antiplatelet medications were associated with presence of TMBs (Table 1). Other cardiovascular risk factors such as hypertension (P = 0.552), diabetes (P = 0.852), stroke (P = 0.405), or anticoagulant (P = 1), antihypertensive (P = 0.229), or lipid lowering (P = 0.066) concomitant medications were not associated with presence or absence of TMBs. Within the population of patients with evidence of punctate and/or linear TMBs, those with or without specifically linear TMBs did not differ for demographic variables including age (P = 0.406), sex (P = 0.702), race (P = 0.112) and ethnicity (P = 0.118) (data not shown). Emergency department intake variables such as GCS at admissions (P = 0.191), trauma level of hospital site (P = 0.270), injury cause (P = 0.446), time from injury to clinical CT (P = 0.655) and time from injury to research MRI (P = 0.411) also did not differ between patients with or without linear TMBs (data not shown). There was also no significant difference in outcome (GOSE; P = 0.973) in those with or without linear TMBs.

More than half of the patients (250/439, 55%) returned for follow-up at 30- or 90-days post-injury. The population with available outcome data was older, white in race, and had a larger fraction of patients with TMBs compared to the population that was lost to follow-up (Supplementary Table 2). Table 2 shows the demographic and clinical features that were predictive of outcome in univariate analysis. Factors including GCS at admission (P = 0.044), clinical diagnosis of TBI (P = 0.014), evidence of injury observed on clinical CT (P = 0.003) and time from injury to start of research MRI (P = 0.001) were significant univariate predictors of outcome, and were included in the binary logistic regression. Age (P = 0.355), sex (P = 0.436), injury cause (P = 0.840) and time from injury to clinical CT (P = 0.537) were not significant univariate predictors of outcome and were not included in the regression. In the binary logistic regression analysis (Supplementary Table 3) presence of both linear and punctate TMBs remained a significant predictor of outcome [β = 0.908, $P < 0.05$; odds ratio (OR) = 2.5]. Trauma-level of hospital site (β = 0.996, $P < 0.05$; OR = 2.7) and time to MRI (β = −0.034, $P < 0.05$; OR = 0.97) were also significant predictors of outcome.

Index neuropathology case: *in vivo* to *ex vivo* imaging characterization of traumatic brain injury

Punctate and curvilinear hypointensities visualized on axial T_2^*-weighted MRI were observed to have linear shape on coronal view (Fig. 2) of index patients acute T_2^*-weighted 3 T MRI. The pattern of hypointensities observed on acute DWI images with corresponding low apparent diffusion coefficient appear to manifest in tissue surrounding punctate TMBs observed on axial T_2^*-weighted magnetic resonance images of the index and mild TBI patient (Fig. 2), indicating cytotoxic oedema in tissue surrounding TMBs. Additional hypointense lesions visualized on FLAIR magnetic resonance images of the index and mild TBI patient, characteristic of vasogenic oedema, co-localize to the same region of tissue where TMBs are observed on axial T_2^*-weighted MRI. Punctate and curvilinear hypointensities visualized on axial T_2^*-weighted MRI were observed to have linear shape on coronal view (Fig. 2) of the index patient's acute T_2^*-weighted 3 T MRI. This pattern of hypointensities observed on acute T_2^*-weighted 3 T MRI taken within 48 h of injury was still visible at 101 days post-injury in the index patient (Fig. 3). These hypointensities were also observed on post-mortem T_2^*-weighted 7 T MRI of the formalin fixed brain. Despite the severe nature of this patient's injury, the linear TMBs observed were similar to those in patients with mild injury (Fig. 2G–L). Linear TMBs observed acutely on the *in vivo* MRI were also visible on the 101 days post-injury *in vivo* MRI and on post-mortem *ex vivo* T_2^*-weighted 7 T MRI of the formalin fixed brain (Fig. 3). Higher resolution *ex vivo* imaging (7 T) revealed that the linear TMBs identified on 3 T *in vivo* MRI were hypointensities that extend from grey matter into white matter with a linear shape.

Post-mortem imaging and histopathological correlates of traumatic brain injury

An MRI-guided strategy was used to target specific regions of interest for tissue sectioning, as described in the methods. Using this approach, regions of the index brain that contained TMBs visible on post-mortem 7 T MRI were accurately aligned with corresponding tissue histology (Fig. 4). TMBs seen on 7 T MRI were co-localized with areas of iron complexed as haemosiderin deposits in macrophages in the perivascular space surrounding a vessel (Fig. 4A–D), which is ~50 μm in diameter. Haemosiderin-laden macrophages were also observed in the perivascular space surrounding smaller

Table 2 Demographic and clinical predictors of outcome

	Total *n* = 250	Good outcome (GOSE 7 and 8) *n* = 147	Disability (GOSE ⩽ 6) *n* = 103	*P*-value	χ^2 (df) / U
Demographics					
Age					
18–30	56 (22%)	29 (20%)	27 (26%)	0.355	2.073 (2)
31–64	150 (60%)	89 (60%)	61 (59%)		
65 +	44 (18%)	29 (20%)	16 (15%)		
Sex					
Male	176 (70%)	100 (68%)	76 (74%)	0.436	1.659 (2)
Race					
White	172 (69%)	113 (77%)	59 (57%)	**0.004**	10.849 (2)
African-American	58 (23%)	25 (17%)	33 (32%)		
Other	20 (8%)	9 (6%)	11 (11%)		
ED intake					
Trauma Level					
Level 1	108 (43%)	45 (31%)	63 (61%)	**0.001**	23.040 (1)
Level 2	142 (57%)	102 (69%)	40 (39%)		
Injury cause					
Road traffic accident	124 (49%)	72 (49%)	52 (50%)	0.840	1.424 (4)
Incidental fall	95 (38%)	55 (37%)	40 (39%)		
Other non-intentional injury	12 (5%)	9 (6%)	3 (3%)		
Violence/assault	17 (7%)	10 (7%)	7 (7%)		
Other	2 (1%)	1 (1%)	1 (1%)		
GCS (*n**)	242	141	101		
15	170 (70.2%)	105 (74%)	65 (64%)	**0.044**	6.265 (2)
14	51 (21.1%)	29 (21%)	22 (22%)		
⩽13	21 (8.7%)	7 (5%)	14 (14%)		
TBI diagnosis					
Mild	211(84%)	131(89%)	80 (78%)	**0.014**	8.480 (2)
Moderate	29 (12%)	14 (10%)	15 (14%)		
Severe	10 (4%)	2 (1%)	8 (8%)		
Clinical CT					
CT	176 (70%)	114 (78%)	62 (60%)	**0.005**	8.756 (1)
Parenchymal haemorrhage	221 (88%)	135 (92%)	86 (83%)	**0.047**	4.110 (1)
Extra axial haemorrhage	180 (72%)	116 (79%)	64 (62%)	**0.004**	8.454 (1)
TMB classification					
Presence of any TMBs	94 (38%)	45 (31%)	49 (48%)	**0.005**	7.425 (1)
Presence of punctate TMBs					
No punctate	176 (70%)	116 (79%)	60 (58%)	**0.001**	17.999 (2)
<5	51 (20%)	26 (18%)	25 (24%)		
⩾5	23 (9%)	5 (3%)	18 (17%)		
Presence of linear TMBs	67 (27%)	32 (22%)	35 (34%)	**0.042**	4.604 (1)
presence of both: linear and punctate TMBs	47 (19%)	19 (13%)	28 (27%)	**0.005**	8.067 (1)
Time from injury to imaging, h, median (Q1–Q3)					
Injury to clinical CT	1.5 (1.1–2.8)	1.5 (1.07–3.0)	1.48 (1.05–2.62)	0.537	7223.5[a]
Injury to research MRI	16.9 (6.8–26.0)	12.12 (5.32–21.45)	20.92 (8.98–31.28)	**0.001**	**5361.5**[a]

GCS at time of arrival to emergency department (ED) was not documented for all patients. Percentages reflect sample size (*n* numbers) reflected in this row. Significance (bold) was determined for any *P*-value that was <0.05. Mann-Whitney for injury to CT and injury to research MRI.

[a]Calculated using non-parametric Mann-Whitney U-test.

vessels distally (Fig. 4B). Collections of haemosiderin-laden macrophages and some free iron were observed between the vessels and neuropil, in the perivascular space of large and small vessels (Fig. 4B–D). Focal loss of the neuropil with significant infiltration by activated macrophages is observed distally to regions of vascular injury. Additionally, we observed capillary proliferation and significant reactive astrocytosis surrounding the loss of neuropil and enlarged perivascular spaces in proximity to injured vessels, both characteristic of ischaemia. Nissl stained sections revealed a loss of cell bodies around linear structures consistent with iron signal co-localized along a vessel. Similarly, Gallyas silver staining showed reduced myelin as well as the absence of axonal injury

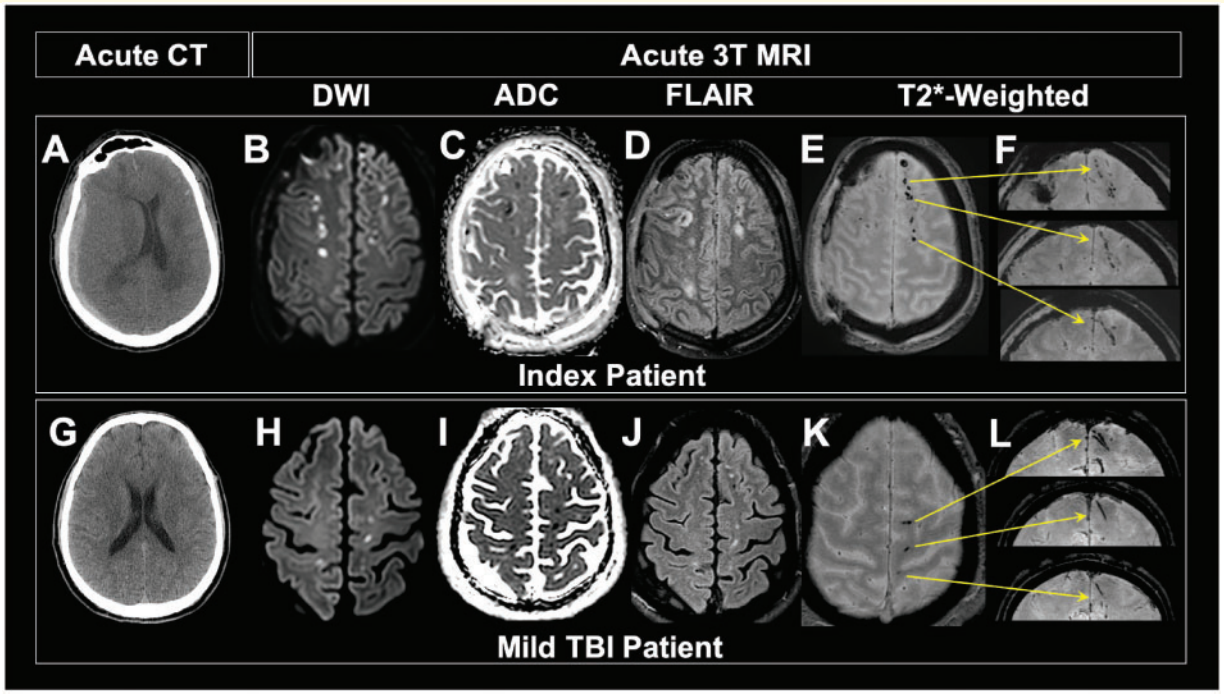

Figure 2 Imaging comparison of mild TBI patient and index patient. (**A**) Acute CT of index patient reveals subdural haemorrhage on patient's right side, showing that the index patient was not of mild severity. (**B**–**F**) Acute 3 T MRI shows pattern of TMBs similar to that of mild TBI patient. (**G**) Acute CT of mild TBI patient in THINC study is unremarkable, showing no extra-axial blood or injury to the parenchyma. Hyperintensity viewed on diffusion-weighted imaging and corresponding hypointensity observed on apparent diffusion coefficient (ADC) of both index (**B** and **C**) and mild TBI patients (**H** and **I**) shows similar patterns of cytotoxic oedema in tissue surrounding TMBs. Pattern of hyperintense signal observed on FLAIR on both the index (**D**) and mild (**J**) TBI patients suggest acute vasogenic oedema around the same areas that we see TMBs. Punctate and curvilinear patterns of hypointensities observed on axial gradient recalled echo (GRE) images of index (**E**) and mild (**K**) TMBs have a linear shape on coronal view in both patients (**F** and **L**). Yellow arrows indicate exact location of each TMB in coronal view. Although not mild, the index patient has similar patterns of linear TMBs as observed in mild TBI patients.

pathology, including a lack of axonal spheroids or beading in the surrounding areas (Fig. 4E–J). In sections targeting TMBs, evidence of axonal injury pathology or axonal spheroids was also absent in haematoxylin and eosin and in APP stained sections (Supplementary Fig. 2). In a region negative for TMB on *in vivo* and *ex vivo* MRI, haematoxylin and eosin and Perls stained sections were also negative for iron-laden macrophages but positive on APP, with occasional APP expression of axonal processes in white matter (Supplementary Fig. 2).

The presence of iron-positive macrophages in 2D histology suggested vascular injury. A 3D volume reconstruction was used to examine the extent of iron-positive macrophages in the perivascular space along the extended vascular tree. High resolution 3D reconstructions of the Perls stained histology sections generated a minimum intensity projection across a stack of digitized serial tissue sections through the tissue block (Fig. 5). The 3D reconstruction contained structures co-localized with iron-laden macrophages. These structures branch and extend over distances of centimetres in a pattern similar to the shape of the vascular tree and the linear TMBs observed on MRI (Fig. 5). Interleaved serial sections of the area of TMBs in tri-planar view revealed a territory of injured vasculature in areas visible on MRI as punctate and linear hypointensities.

Discussion

This work provides evidence that: (i) TMBs have a high prevalence in acute TBI, being identified in 31% of patients in our predominantly mild population; (ii) within those who had presence of TMBs, there were no significant demographic or clinical predictors between those who had linear TMBs versus those who did not; (iii) both punctate and linear TMBs are predictive of outcome; those with evidence of TMBs were twice as likely to have disability at 30- or 90-days post-injury; (iv) across injury severity, some punctate TMBs visualized on axial T_2*-weighted imaging were often revealed as linear structures in the coronal plane; and (v) after co-localizing TMBs seen on *in vivo* MRI and post-mortem high-resolution MRI to histopathology, we found iron-laden macrophages in the perivascular space surrounding injured vasculature, suggesting TMBs are a form of traumatic vascular injury.

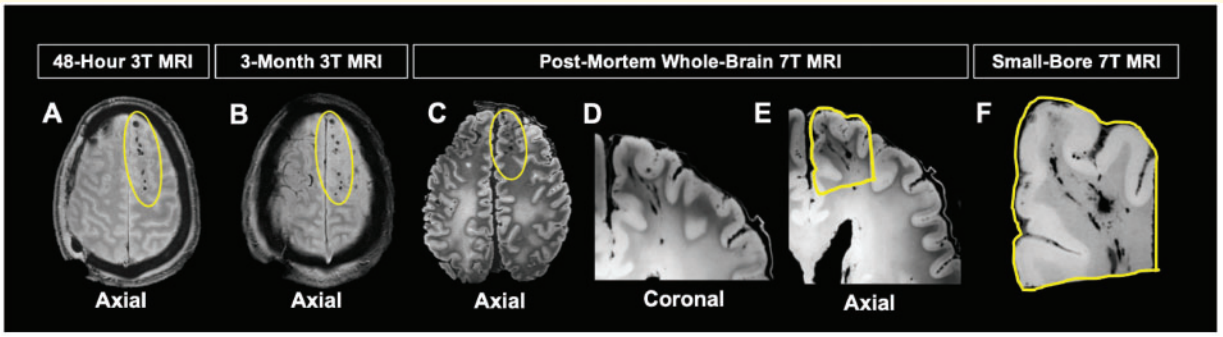

Figure 3 Evolution of TMBs in index patient. (**A**) Acute T_2^*-weighted 3 T MRI obtained within 48 h of injury shows pattern of TMBs (within yellow oval) consistent with T_2^*-weighted 3 T MRI obtained 3 months post injury (**B**), the last MRI obtained. The patient died ~7 months post-injury. (**C**) Post-mortem T_2^*-weighted 7 T MRI showed TMBs remained stable from acute *in vivo* MRI to post-mortem MRI, with some morphology changes from brain extraction. Pattern of linear TMBs observed on post-mortem coronal (**D**) and axial (**E**) images of the whole brain. Region targeted for histopathological analysis outlined in yellow (**E**). (**F**) High-resolution small-bore 7 T MRI of targeted region to confirm TMB imaging within tissue prior to embedding region of interest for histological co-localization of TMB.

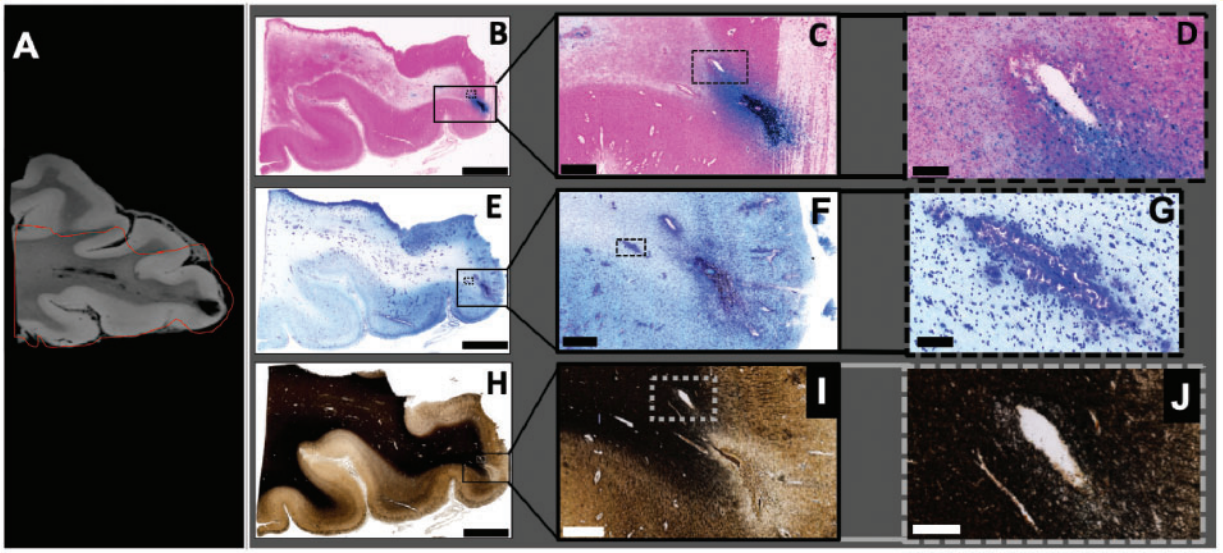

Figure 4 MRI guided pathology shows evidence of injury to the vasculature. (**A**) 7 T small-bore 3D T_2^*-weighted MRI scan of region with visible TMBs within the index case. Red line indicates outline of the region that was included within the tissue block for 20-μm thick histology sections. (**B**–**D**) Perls Prussian Blue stain shows iron deposits in haemosiderin-laden macrophages. Solid line box (**B**) includes the grey-white matter junction and indicates the enlarged region shown in **C**. Dotted line box (**C**) indicates enlarged region in **D** showing cellular detail. (**E**–**G**) Nissl cytological stain. Solid line box (**E**) indicates enlarged region shown in **F**. Dotted line box (**F**) indicates enlarged region in **G** showing a linear pattern of high cell density. (**H**–**J**) Gallyas silver stain for myelin. Solid line box (**H**) indicates enlarged section shown in **I**. Grey dotted line box (**H**) shows grey-white matter border and indicates enlarged section in **I**. Within the white matter, myelin is absent from a linear region (**I**). In the adjacent area, myelin is slightly reduced (**J**) and cells with iron deposits are present (**D**). Scale bars in **B**, **E** and **H** = 3 mm; **C** and **F** = 500 μm; **D** and **I** = 100 μm; **G** = 50 μm; **J** = 30 μm.

TMBs are a common finding on MRIs of patients following TBI. The field currently associates TMBs to both severe injury and clinical outcomes (Babikian *et al.*, 2005; Colbert *et al.*, 2010; Beauchamp *et al.*, 2013; Yuh *et al.*, 2013; Izzy *et al.*, 2017). However, our data suggest that TMBs are not exclusive to moderate or severe TBI. We have identified TMBs in 27% of mild, 47% of moderate, and 58% of severe TBI patients. We found that patients with TMBs had more severe injury and lower GCS compared to patients without TMBs. While our results are consistent with other studies demonstrating a positive relationship between TMB prevalence and injury severity, we also found that TMBs are present in more than one quarter of our mild TBI patients. This finding is important because most studies on TMBs are conducted on patients with severe injury. Thus, TMBs are observed more frequently in patients

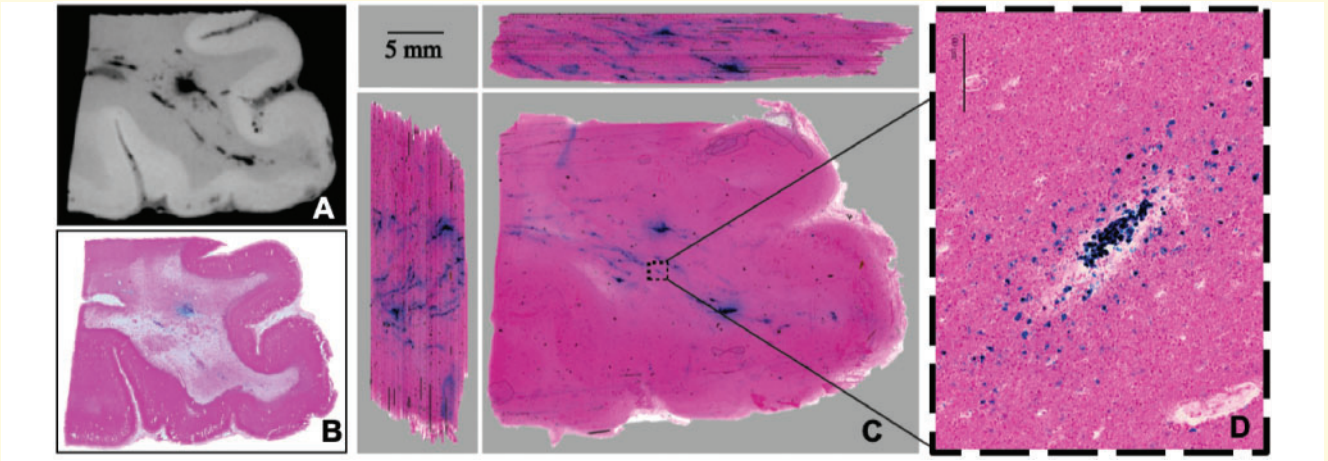

Figure 5 Pathology underlying TMBs: injury to the vasculature. (**A**) High-resolution 7 T MRI of tissue block containing region of interest co-localized to TMBs observed *in vivo* and *ex vivo* whole-brain MRI. (**B**) Standard 2D histopathology section (20-μm thick) from the imaged tissue block (**A**) stained with Perls Prussian Blue reveals iron in macrophages surrounding a large vessel. (**C**) Serially cut tissue sections digitized as a 3D volume, shown as side views in the adjacent panels. A 3D minimum intensity projection (MIP) image of the Perls stained histology reconstructed to match high-resolution 7 T MRI (**A**). (**C**) 3D reconstruction of interleaved tissue sections stained for iron deposits demonstrates iron laden macrophages that are connected and branching over centimetres of tissue. (**D**) Enlarged section of (**C**) showing iron-laden macrophages that co-localized with a vessel. These interleaved serial sections of the TMB in tri-planar view reveal a territory of injured vasculature in areas visible on MRI as punctate or linear hypointensities. Injury to the large vessel is indicated by confluent regions of iron-laden macrophages that create sufficient signal for detection on MRI. Injury to some of the other smaller vessels is only detected on post-mortem histology in a 3D reconstruction. The tri-planar view and high resolution identifies connectivity of the injured vessels ranging from large to small diameters.

with severe injury (Geurts *et al.*, 2012; Riedy *et al.*, 2016; Toth *et al.*, 2016), which has made it difficult to determine if TMBs alone can predict clinical outcome.

To investigate the clinical implications of TMBs further, we controlled for variables that are known to predict poor outcome (trauma level and trauma-related injury on CT) and found that TMBs were a significant independent predictor of outcome. Patients with evidence of both punctate and linear TMBs were twice as likely to have disability (GOSE $\leqslant$ 6) on follow-up. We defined good recovery as GOSE of 7 (lower good recovery) and 8 (upper good recovery) and poor recovery of $\leqslant$6 (upper moderate disability to death). Yuh and colleagues (2013) similarly found that TMBs were a significant predictor of poor outcome, although they defined good outcome to be GOSE of 8 and poor outcome as GOSE of $\leqslant$7. They also found an association between number of lesions and outcome, with patients having $\geqslant$4 TMBs three times as likely to have poor outcome compared to patients with $\leqslant$3 TMBs. Others similarly found an association between lesion load and clinical outcome (Spitz *et al.*, 2013). However, we found that multiple punctate TMBs seen in TBI patients at 3 T were visible in connected branching structures. Thus, perhaps the effect of lesion load may be attributed to double counting of the same injured vascular network.

Identifying the cellular changes responsible for hypointensities observed on T_2^*-weighted images is critical for discovering primary injury mechanisms and ultimately clinical significance. To date, identification of TMBs on gross pathology alone has been challenging (Tatsumi *et al.*, 2008). Post-mortem pathology studies of patients with severe TBI have established a link between evidence of direct injury to the axons not visible on neuroimaging and punctate hypointense lesions seen on T_2^*-weighted MRI, particularly in the corpus callosum and the infratentorial structures (Adams *et al.*, 1982; Onaya, 2002; Keene *et al.*, 2018). With recent interest in mild TBI, there has been a tendency to equate TMBs in mild patients with underlying axonal injury, although the evidence in the literature supporting this assertion remains ambiguous.

This study presents the application of MRI-guided pathology to investigate specific TBI-associated lesions. This direct radiological-pathological correlation of *in vivo* and *ex vivo* imaging presented a unique opportunity to characterize TBI-related lesions seen acutely (within 48 h) after injury and further characterize the morphology associated with those lesions with targeted histology. Specifically, we identified that microbleeds evident within 48 h of TBI remained stable for at least 100 days after injury on *in vivo* MRIs. The presence of microbleeds in the same area of the cortex on post-mortem 7 T MRIs signified that microbleeds seen *in vivo* are also observed *ex vivo*. Hypointensities on T_2^*-weighted images, tracking through grey to white matter, appeared blue on Perls Prussian blue staining and correspond to iron in haemosiderin deposits that form in macrophages in the perivascular space tracking along vessels. Most iron was observed in macrophages outside of the parenchyma, suggesting iron (blood) was extravasated outside of injured vessels. Nissl- and myelin-stained sections of the same region of interest revealed fewer cell bodies and

reduced myelin in the area of the injury, consistent with cell loss and demyelination. This indicates that the parenchyma surrounding the vessel is also injured. Further, on haematoxylin and eosin- and Nissl-stained regions located distally to and surrounding the injured vasculature, we observed focal loss of the neuropil with significant infiltration by activated macrophages and enlarged perivascular spaces. Both pathologies are characteristic of ischaemia, and correlate to regions where we observe cytotoxic and vasogenic oedema on *in vivo* acute MRI. Visualizing TMBs on 3D reconstruction of 2D Prussian blue histology, we observed macrophages along small and large vessels throughout the vasculature, suggesting a linear structure that appears to be an injury not just to a single large vessel but to a vascular tree. Evidence of axonal injury was not observed in these co-localized sections. Histological examination revealed a more extensive territory of vascular damage as compared to what was observed in small-bore 7 T MRI.

Using MRI guided pathology, we identified that what appeared as a punctate TMB on MRI corresponds to iron-laden macrophages in the perivascular space surrounding a vascular tree that extends over centimetres. This was surprising, as based upon the small-bore 7 T MRI, we expected to see iron within the parenchyma; however, we found iron inside macrophages outside of the parenchyma between the vessel and neuropil, tracking alongside vessels. This signifies that the extent of injury is more extensive than indicated on MRI, which has consequences to cellular function over a larger area of brain. Our findings also suggest that punctate and linear TMBs may not be distinct entities, but the difference in shape may be an issue of resolution. This presents evidence in support of a vascular injury, as depicted in Fig. 5. The mechanism of this injury could be due to parasagittal bridging veins and other vessels anchored to the meninges that are directly injured from the movement of the brain within the skull, leading to secondary brain injury, as depicted in Fig. 6.

Our observations of vascular injury on *in vivo* and *ex vivo* MRI and in the underlying histopathology are consistent with and build on early pathological investigations of TBI. Historically, observations of what are now referred to as TMBs suggested that they may be due to underlying vascular injury (Oppenheimer, 1968; Tomlinson, 1970). Post-mortem reports showing microscopic lesions in TBI patients have shown similar microglial clusters that are commonly found along a blood vessel, suggesting that these lesions are due to stretching and tearing of small vessels leading to tiny capillary haemorrhages (Oppenheimer, 1968). Later studies, often in severe patients, have ascribed these findings as secondary to the focal shearing of axons resulting in diffuse axonal injury (Adams *et al.*, 1982; Scheid *et al.*, 2003, 2006; Babikian *et al.*, 2005). Even more recent studies in animals and humans have shown a connection of the signal abnormalities observed on T_2^*-weighted MRI to injury to the vasculature (Iwamura *et al.*, 2012; Glushakova *et al.*, 2014; Kenney *et al.*, 2016; Tagge *et al.*, 2018) suggesting the injury causes tearing to the blood vessels and triggering bridging veins to rupture. Thus, some groups have speculated cerebrovascular pathology to be a mechanistic link between TBI and Alzheimer's disease (Ramos-Cejudo *et al.*, 2018). In the post-mortem analysis of human brains from individuals with a history of multiple TBI's, researchers commonly observe neurofibrillary tangles surrounding penetrating small cortical vessels (McKee *et al.*, 2013, 2015) and identify it as a characteristic pathology of chronic traumatic encephalopathy. Interestingly, these pathologies appear as linear

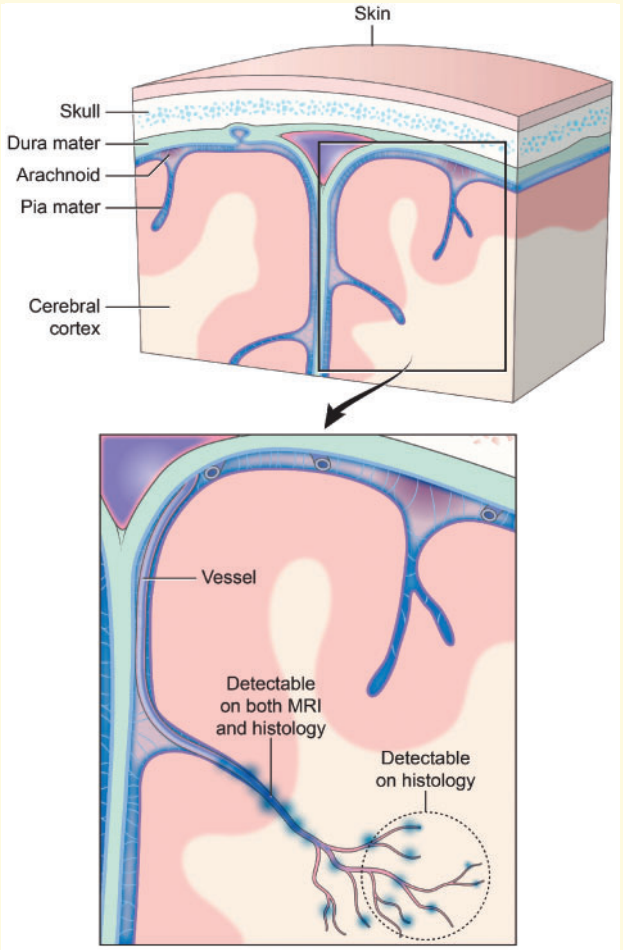

Figure 6 Traumatic vascular injury. Traditionally, TMBs have been described as markers for diffuse axonal injury. However, TMBs have not been characterized as a form of traumatic vascular injury. MRI and 3D histology identified an underlying pathology of TMBs to be an injury to not just a single vessel, but injury that extends to a vascular network. Injury to a large blood vessel causes iron deposition that is detectable on *in vivo* and *ex vivo* MRI (at 3 T and 7 T). Smaller vessels that form a broader vascular network with the larger vessels are missed in these magnetic resonance images. High-resolution 3D histology of iron deposits in macrophages identified more extensive vascular injury involving smaller vessels that connect to the larger injured vessel detected on MRI. The schematic above illustrates a model of this vascular injury pattern and potential levels of detection with MRI and histological approaches.

accumulations that extend from the surface of the brain to the grey-white junction and, on cross-sectional visualization, are observed as 'dot-shaped' or 'thread-like' clusters (McKee *et al.*, 2013, 2015). We report haemosiderin-laden macrophages around penetrating vessels and microvessels that are visualized in similar shapes and manifestations.

The presence of TMBs may be a biomarker for vascular-related interventions after TBI. The leakage of blood from damaged blood vessels can trigger an inflammatory response. Researchers have previously suggested that TMBs result from chronic blood–brain barrier disruption and delayed chronic microvascular damage, which produce toxic iron deposition and initiate continued neuroinflammation and demyelination of axons (Harting *et al.*, 2008; Glushakova *et al.*, 2014). In addition to the damaged vessels themselves, the disruption of normal pathways of blood flow and the influx of inflammatory cells could result in secondary injury to the brain tissue as a result of ischaemia. We have shown *in vivo* acute MRI data of cytotoxic and vasogenic oedema surrounding TMBs, and post-mortem pathology data of focal loss of neuropil, infiltrating macrophages and enlarged perivascular spaces proximal to injured vasculature, indicative of secondary injury to the brain tissue surrounding vascular injury. Our data suggest that acute TMBs are associated with acute MRI diffusion-weighted changes like those well-described from acute stroke studies. Thus, we postulate that TMBs may be useful biomarkers for identifying TBI patients that may benefit in the acute phase from therapies aimed at minimizing acute ischaemic damage, or in the chronic phase, at improving microvascular cerebral blood flow (Zhang *et al.*, 2006; Kenney *et al.*, 2018). The persistence of inflammatory cells triggered by these TMBs in the perivascular spaces may also impede fluid movement, which, if in humans is analogous to the glymphatic system critical for removing substrates from the brain as described in rodents (Glushakova *et al.*, 2014), may affect the build-up of substrates and lead to secondary injury in humans as well. TMBs may also serve as biomarkers for patients more likely to have these glymphatic flow system disruptions, facilitating the identification of appropriate patients for therapeutic clinical trials. For example, pharmacological agents suggested by other TBI investigators to act on the microvasculature to increase cerebral perfusion include sildenafil (Kenney *et al.*, 2018) and beta blockers such as propranolol (Loftus *et al.*, 2016). In contrast, minocycline has the potential to reduce acute ischaemic injury through its effects on inflammation, blood–brain barrier, and oedema (Mizuma and Yenari, 2017).

Our MRI guided pathology methods address the limitations of standard pathological analysis of TMBs by improving the detection on histology, identifying the underlying pathophysiology, and providing confidence in linking the mechanism of injury to radiological findings. This radiological-pathological analysis shows that what was previously considered as punctate on 3 T *in vivo* MRI appears to have a linear shape using high-resolution 7 T MRI, suggesting that punctate and linear TMBs may be the same vascular injury. The ability to unambiguously co-localize the same region of injury on imaging within interleaved serial section histology allowed us to identify and better visualize the extent of injury to the vasculature. The microscopic sequelae of TBI were more extensive than could be seen by conventional *in vivo* imaging.

There are some limitations to this study. The methodology used here tended a conservative rating of the presence and classification of TMBs. It is possible that a greater number or different classification would occur if one sequence was considered (SWI or GRE) blinded to the other sequences. We believe, however, a comprehensive review of the imaging study is more representative of how images are interpreted in routine clinical practice.

There is always potential for selection bias. It is not clear if the enrolled population is representative of all patients presenting to the emergency department with similar characteristics. Because study staff were not available 24-7, it is likely that patients discharged rapidly from the emergency department are underrepresented. Similarly, patients with greater severity of injury (head or polytrauma) or unable to provide self-consent are likely underrepresented. Further work is needed to estimate prevalence. The population (Table 2) returning for follow-up is slightly different than the population who did not return (Supplementary Table 1). Patients who were more severely injured, and with a greater number of TMBs, were more likely to return for follow-up compared to those who did not return. This could be indicative that the follow-up patients are representative of more symptomatic patients, and thus may indicate a selection bias. However, other groups have also reported greater attrition that did not appear to impact their correlation of TMBs with clinical outcome (Liu *et al.*, 2016). Additionally, our study is limited to a single outcome variable. The GOSE is not capable of capturing subtle post-concussive symptoms. However, for the purposes of this study, it is reliable for identifying patients who have not recovered and have persistent debilitating symptoms. The GOSE is commonly used as the sole clinical outcome variable in clinical TBI studies (Scheid *et al.*, 2003; Geurts *et al.*, 2012; Liu *et al.*, 2016). The choice of GOSE as the primary clinical outcome is an oversimplification of the clinical sequela, including the impact of the injury on cognition. The lack of cognitive outcome measures limit the interpretability of the impact of TMB on more subtle function that may not be reflected in the global measure such as the GOSE. Future studies should include a range of outcome variables to investigate more subtle symptoms. Lastly, our pathological analysis is limited to one index patient who had a complicated clinical history and severe injury with subdural haemorrhage. While this is not ideal, our serial *in vivo* imaging protocol allows us to be confident that the observed TMBs are the result of the acute injury and remain stable from the chronic to post-mortem period. The TMBs in the index patient were on the contralateral side to the subdural haemorrhage and had the same pattern

observed on the magnetic resonance images of mild patients. Clearly, future studies are needed to examine the pathophysiology of TMBs and cerebral microbleeds that are not trauma-related.

In conclusion, this study provides evidence that TMBs represent traumatic vascular injury, which is not exclusive to severe injury and is predictive of outcome. Of the 439 TBI patients in our population, 134 (30.5%) patients were positive for TMBs. Of the TMB positive population, 97 (72%) were mild TBI patients. After controlling for trauma-related confounding variables, we found that TMBs were a significant predictor of outcome. Patients with TMBs were twice as likely to have disability, with a GOSE of $\leqslant 6$ on follow-up. This study also addresses the current debate of the underlying pathophysiology of TMBs. Based on current literature we expected to find axonal injury in sections corresponding with TMBs. While we found evidence of cell loss and demyelination on our histopathological analysis, findings such as axonal bulbs or APP-positive axonal processes consistent with axonal injury were not observed in TMB-positive sections. Using MRI-guided pathology, we identified that what appeared as a punctate TMB on MRI corresponds to iron-laden macrophages in the perivascular space surrounding a vascular tree that extends over centimetres. These patterns likely represent traumatic injury to the microvasculature, resulting in extravasation of erythrocytes into perivascular spaces along vascular trees. While we cannot rule out that patients with TMBs have co-existing diffuse axonal injury, we do conclude that traumatic vascular injury is a distinct phenotype of TMBs and may provide opportunities for new therapies.

Acknowledgements

We would like to acknowledge Dr Mark D. Whiting for providing technical editing and proofreading; Dr John L. Ostuni for technical assistance with the 3D printed brain holder/slicer; Dr Pascal Santi for technical support with high-resolution T_2^*-weighted 7T MRI sequence; Allison Dempsey for her assistance with histology. We thank the patients and families for their willingness and generosity to participate in this study.

Funding

This work was supported by the Department of Defense in the Center for Neuroscience and Regenerative Medicine, the Intramural Research Programs at the NIH Clinical Center and NINDS, the Crick-Clay Professorship and the Mathers Foundation. The contents of this article are solely the responsibility of the authors and do not represent the official views of the Department of Defense or the Center for Neuroscience and Regenerative Medicine.

Competing interests

The authors declare no competing financial or non-financial interests.

Supplementary material

Supplementary material is available at *Brain* online.

References

Absinta M, Nair G, Filippi M, Ray-Chaudhury A, Reyes-Mantilla MI, Pardo CA, et al. Postmortem magnetic resonance imaging to guide the pathologic cut: individualized, 3-dimensionally printed cutting boxes for fixed brains. J Neuropathol Exp Neurol 2014; 73: 780–8.

Adams JH, Graham DI, Murray LS, Scott G. Diffuse axonal injury due to nonmissle head injury in humans: an analysis of 45 cases. Ann Neurol 1982; 12: 557–63.

Babikian T, Freier MC, Tong KA, Nickerson JP, Wall CJ, Holshouser BA, et al. Susceptibility weighted imaging: neuropsychologic outcome and pediatric head injury. Pediatr Neurol 2005; 33: 184–94.

Beauchamp MH, Beare R, Ditchfield M, Coleman L, Babl FE, Kean M, et al. Susceptibility weighted imaging and its relationship to outcome after pediatric traumatic brain injury. Cortex 2013; 49: 591–8.

Colbert CA, Holshouser BA, Aaen GS, Sheridan C, Oyoyo U, Kido D, et al. Value of cerebral microhemorrhages detected with susceptibility-weighted MR imaging for prediction of long-term outcome in children with nonaccidental trauma. Radiology 2010; 256: 898–905.

Conijn MM, Geerlings MI, Biessels GJ, Takahara T, Witkamp TD, Zwanenburg JJ, et al. Cerebral microbleeds on MR imaging: comparison between 1.5 and 7T. AJNR Am J Neuroradiol 2011; 32: 1043–9.

Cota MR, Moses AD, Jikaria NR, Bittner KC, Diaz-Arrastia RR, Latour LL, et al. Discordance between documented criteria and documented diagnosis of traumatic brain injury in the emergency department. J Neurotrauma 2018; 36: 1335–42.

Fisher M, French S, Ji P, Kim RC. Cerebral microbleeds in the elderly: a pathological analysis. Stroke 2010; 41: 2782–5.

Geurts BHJ, Andriessen TMJC, Goraj BM, Vos PE. The reliability of magnetic resonance imaging in traumatic brain injury lesion detection. Brain Inj 2012; 26: 1439–50.

Glushakova OY, Johnson D, Hayes RL. Delayed increases in microvascular pathology after experimental traumatic brain injury are associated with prolonged inflammation, blood–brain barrier disruption, and progressive white matter damage. J Neurotrauma 2014; 31: 1180–93.

Harting MT, Jimenez F, Adams SD, Mercer DW, Cox CS Jr. Acute, regional inflammatory response after traumatic brain injury: Implications for cellular therapy. Surgery 2008; 144: 803–13.

Huang YL, Tseng YC, Chen DYT, Hsu HL, Chen CJ. Susceptibility-weighted MRI in mild traumatic brain injury: the importance of cerebral microbleeds. J Neurol Neurophysiol 2015; 6: 321.

Iwamura A, Taoka T, Fukusumi A, Sakamoto M, Miyasaka T, Ochi T, et al. Diffuse vascular injury: convergent-type hemorrhage in the supratentorial white matter on susceptibility-weighted image in cases of severe traumatic brain damage. Neuroradiology 2012; 54: 335–43.

Izzy S, Mazwi NL, Martinez S, Spencer CA, Klein JP, Parikh G, et al. Revisiting grade 3 diffuse axonal injury: not all brainstem microbleeds are prognostically equal. Neurocrit Care 2017; 27: 199–207.

Keene CD, Latimer CS, Steele LM, Mac Donald CL. First confirmed case of chronic traumatic encephalopathy in a professional bull rider. Acta Neuropathol 2018; 135: 303–5.

Kenney K, Amyot F, Haber M, Pronger A, Bogoslovsky T, Moore C, et al. Cerebral vascular injury in traumatic brain injury. Exp Neurol 2016; 275: 353–66.

Kenney K, Amyot F, Moore C, Haber M, Turtzo LC, Shenouda C, et al. Phosphodiesterase-5 inhibition potentiates cerebrovascular reactivity in chronic traumatic brain injury. Ann Clin Transl Neurol 2018; 5: 418–28.

Lawrence TP, Pretorius PM, Ezra M, Cadoux-Hudson T, Voets NL. Early detection of cerebral microbleeds following traumatic brain injury using MRI in the hyper-acute phase. Neurosci Lett 2017; 655: 143–50.

Lee BC, Tward DJ, Mitra PP, Miller MI. On variational solutions for whole brain serial-section histology using a Sobolev prior in the computational anatomy random orbit model. PLoS Comput Biol 2018; 14: 1–20.

Liu J, Kou Z, Tian Y. Diffuse axonal injury after traumatic cerebral microbleeds: an evaluation of imaging techniques. Neural Regen Res 2014; 9: 1222.

Liu W, Soderlund K, Senseney JS, Joy D, Ollinger J, Wang Y, et al. Imaging cerebral microhemorrhages in military service members with chronic traumatic brain injury. Neuroradiology 2016; 278: 536–45.

Loftus TJ, Efron PA, Moldawer LL, Mohr AM. β-Blockade use for traumatic injuries and immunomodulation. Shock 2016; 46: 341–51.

McKee AC, Stein TD, Kiernan PT, Alvarez VE. The neuropathology of chronic traumatic encephalopathy. Brain Pathol 2015; 25: 350–64.

McKee AC, Stein TD, Nowinski CJ, Stern RA, Daneshvar DH, Alvarez VE, et al. The spectrum of disease in chronic traumatic encephalopathy. Brain 2013; 136: 43–64.

Menon DK, Schwab K, Wright DW, Maas AI. Position statement: definition of traumatic brain injury. Arch Phys Med Rehabil 2010; 91: 1637–40.

Mizuma A, Yenari M. Anti-inflammatory targets for the treatment of reperfusion injury in stroke. Front Neurol 2017; 8: 1–20.

Naka EW, Kajikawa H, Kohriyama T, Nomura H, Mimori Y, Nakamura S, et al. Frequency of asymptomatic microbleeds on T2*-weighted MR images of patients with recurrent stroke: association with combination of stroke subtypes and leukoaraiosis. Am J Neuroradiol 2004; 25: 714–9.

Onaya M. Neuropathological investigation of cerebral white matter lesions caused by closed head injury. Neuropathology 2002; 22: 243–51.

Oppenheimer DR. Microscopic lesions in the brain following head injury. J Neurol Neurosurg Psychiatry 1968; 31: 299–306.

Pinskiy V, Jones J, Tolpygo AS, Franciotti N, Weber K, Mitra PP. High-throughput method of whole-brain sectioning, using the tape-transfer technique. PLoS One 2015; 10: e0102363.

Ramos-Cejudo J, Wisniewski T, Marmar C, Zetterberg H, Blennow K, de Leon MJ, et al. Traumatic brain injury and Alzheimer's disease: the cerebrovascular link. EBioMedicine 2018; 28: 21–30.

Ricciardi CM, Bokkers RPH, Butman JA, Hammoud DA, Pham DL, Warach S, et al. Trauma-specific brain abnormalities in suspected mild traumatic brain injury patients identified in the first 48 hours after injury: a blinded magnetic resonance imaging comparative study including suspected acute minor stroke patients. J Neurotrauma 2017; 34: 23–30.

Riedy G, Senseney JS, Liu W, Ollinger J, Sham E, Krapiva P, et al. Findings from structural MR imaging in military traumatic brain injury. Radiology 2016; 279: 207–15.

Scheid R, Preul C, Gruber O, Wiggins C, Von Cramon DY. Diffuse axonal injury associated with chronic traumatic brain injury: evidence from T2*-weighted gradient-echo imaging at 3T. Am J Neuroradiol 2003; 24: 1049–56.

Scheid R, Walther K, Guthke T, Preul C, von Cramon DY. Cognitive sequelae of diffuse axonal injury. Arch Neurol 2006; 63: 418–24.

Selassie AW, Zaloshnja E, Langlois JA, Miller T, Jones P, Steiner C. Incidence of long-term disability following traumatic brain injury hospitalization, United States, 2003. J Head Trauma Rehabil 2008; 23: 123–31.

Spitz G, Maller JJ, Ng A, O'Sullivan R, Ferris NJ, Ponsford JL. Detecting lesions after traumatic brain injury using susceptibility weighted imaging: a comparison with fluid-attenuated inversion recovery and correlation with clinical outcome. J Neurotrauma 2013; 30: 2038–50.

Tagge CA, Fisher AM, Minaeva OV, Gaudreau-Balderrama A, Moncaster JA, Zhang X-L, et al. Concussion, microvascular injury, and early tauopathy in young athletes after impact head injury and an impact concussion mouse model. Brain 2018; 141: 422–58.

Tatsumi S, Shinohara M, Yamamoto T. Direct comparison of histology of microbleeds with postmortem MR images. Cerebrovasc Dis 2008; 26: 142–6.

Taylor CA, Bell JM, Breiding MJ, Xu L. Traumatic Brain Injury–Related Emergency Department Visits, Hospitalizations, and Deaths—United States, 2007 and 2013. MMWR Surveill Summ 2017; 66: 1–16.

Thurman DJ, Alverson C, Dunn KA, Guerrero J, Sniezek JE. Traumatic brain injury in the United States: a public health perspective introduction: the public health significance of traumatic brain injury. J Head Trauma Rehabil 1999; 14: 602–15.

Tomlinson BE. Brain-stem lesions after head injury. J Clin Pathol Suppl. (R Coll Pathol) 1970; 4: 154.

Tong KA, Ashwal S, Holshouser BA, Shutter LA, Herigault G, Haacke EM, et al. Hemorrhagic shearing lesions in children and adolescents with posttraumatic diffuse axonal injury: improved detection and initial results. Radiology 2003; 227: 322–39.

Toth A, Kovacs N, Tamas V, Kornyei B, Nagy M, Horvath A, et al. Microbleeds may expand acutely after traumatic brain injury. Neurosci Lett 2016; 617: 207–12.

Turtzo LC, Budde MD, Gold EM, Lewis BK, Janes L, Yarnell A, et al. The evolution of traumatic brain injury in a rat focal contusion model. NMR Biomed 2013; 26: 468–79.

Van Veluw SJ, Biessels GJ, Luijten PR, Zwanenburg JJM. Assessing cortical cerebral microinfarcts on high resolution MR images. JoVE (Journal Vis Exp) 2015; 105: e53125.

Van Veluw SJ, Zwanenburg JJM, Engelen-Lee J, Spliet WGM, Hendrikse J, Luijten PR, et al. In vivo detection of cerebral cortical microinfarcts with high-resolution 7T MRI. J Cereb Blood Flow Metab 2013; 33: 322–9.

Yuh EL, Mukherjee P, Lingsma HF, Yue JK, Ferguson AR, Gordon WA, et al. Magnetic resonance imaging improves 3-month outcome prediction in mild traumatic brain injury. Ann Neurol 2013; 73: 224–35.

Zaloshnja E, Miller T, Langlois JA, Selassie AW. Prevalence of long-term disability from traumatic brain injury in the civilian population of the United States, 2005. J Head Trauma Rehabil 2008; 23: 394–400.

Zhang RLZ, Zhang Z, Zhang L, Wang Y, Zhang C, Chopp M. Delayed treatment with sildenafil enhances neurogenesis and improves functional recovery in aged rats after focal cerebral ischemia. J Neurosci Res 2006; 83: 1213–9.